



EFFECTS OF SEDIMENTARY LAYERS ON DIRECTIVITY PULSE AND FLING STEP

Yoshiaki HISADA¹ and Jacobo BIELAK²

SUMMARY

Effects of sedimentary layers on the long-period directivity pulse and the fling step are investigated using the theoretical method developed by Hisada and Bielak [1]. First, basic physics of the directivity pulses and the fling step are investigated using a simple strike-slip fault model in a homogeneous half-space. Next, the method is applied to the strong motion recorded at the Lucerne valley during the 1992 Landers earthquake, using the fault model and the local layered structure model by Wald and Heaton [2]. It was confirmed that the maximum amplitude of the velocity and displacement was inclined to the fault plane at 30 – 50 degree due to the combined effect of the long-period pulse and the fling. The inclusion of sedimentary layers increases greatly both amplitudes and durations of the directivity pulses, whereas it does not affect those of the slip pulses. This is because the directivity pulses are the body and surface waves excited in the sedimentary layers from wide range of faults (the nearest fault to the furthest fault), whereas the fling steps are generated by the slip of the nearest surface fault.

INTRODUCTION

The long-period directivity pulse and the fling step are probably the most important near-source strong ground motions in earthquake engineering (e.g., Somerville *et al.* [3]; Abrahamson [4]). The directivity pulses, as seen in the 1994 Northridge and 1995 Kobe earthquake, have destructive effects on short- to medium-period structures, whereas the fling steps, as seen in the 1992 Landers and 1999 Chi-Chi earthquakes, may have destructive effects on long-period structures, such as high-rise and base-isolated structures. As an example showing the fling step, Fig. 1 shows velocity response spectra ($h=5\%$) for the 1992 Landers and 1999 Chi-Chi earthquakes. Their amplitudes exceed constant level of the velocities of

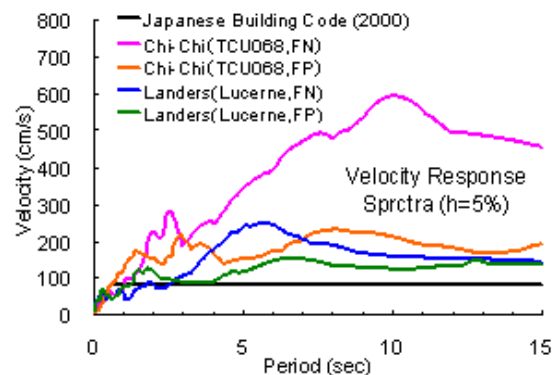


Fig. 1 Examples of the velocity response spectra showing the fling steps

¹ Department of Architecture, Kogakuin University

² Department of Civil & Environmental Engineering, Carnegie Mellon University

building codes (80 to 100 cm/s) at longer periods.

Recently, we developed an efficient method for simulating near-fault strong ground motions in layered media (Hisada and Bielak, [1]); the method rigorously evaluates the dynamic and static terms of Green's functions of layered half-spaces for efficiently computing near-fault strong motions. We first introduce the formulation of the method, and show basic physics of the directivity pulses and the fling step using a simple strike-slip fault model in a homogeneous space. Then, we apply the method to the near-fault strong motion recorded at the Lucerne valley for the 1992 Landers earthquake to investigate the effects of the sedimentary layers on the directivity pulses and the fling steps.

THEORETICAL METHOD FOR SIMULATING NEAR-FAULT STRONG MOTIONS, AND PHYSICAL INTEPRETATION OF DIRECTIVITY PULSE AND FLING STEP

Theoretical Method for Efficiently Simulating Near-Fault Strong Motions

In order to simulate theoretical strong ground motions for near-faults, Hisada and Bielak [1] introduced an efficient method using the following new representation theorem, which evaluates the fault integration of the dynamic and static terms, separately,

$$U_k(Y; \omega) = \int_S \{T_{ik}^D(X, Y; \omega) - T_{ik}^S(X, Y)\} D_i(X; \omega) dS + \int_S T_{ik}^S(X, Y) D_i(X; \omega) dS \dots \dots \dots (1)$$

where, U_k is the k th component of displacement in the Cartesian coordinate system, X and Y are an observation and a source point on the fault plane, respectively, S is the fault plane, D_i is the i th component of the fault slip, and T_{ik}^D and T_{ik}^S are the dynamic and static traction Green's functions of layered half-spaces.

Equation (1) simulates near-fault ground motions much more efficiently than the original representation theorem, which is represented by the total traction Green's function alone. The original theorem requires a lot of CPU time to evaluate the near-singularities of the dynamic Green's function numerically, which show extremely sharp peaks centered at the source point, as shown in Fig.2. By contrast, the first integral of equation (1), in which the static Green's function is subtracted from the dynamic function, can eliminate the near-singularities completely, because the static function includes all the sources of the singularities of the dynamic function. The near singularities appear only in the second integral of equation (1). The evaluation of this integral necessitates that a dense set of integration points be distributed in the neighborhood of the observation point (Fig. 2); this uses up some CPU time. However, since the values of the static functions remain invariant for all frequencies, this integration needs to be done only once.

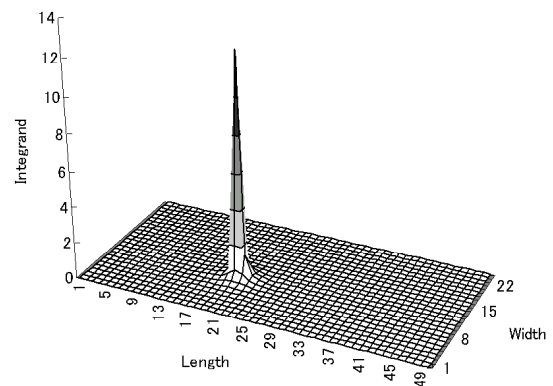


Fig. 2 An example of the near-singularity of an integrand of fault integration.

When we model surface faulting, we need to compute a lot of Green's functions with the source points on and near free surface. For these cases, the wavenumber integrations of Green's functions require a lot of CPU time, because the integrands do not converge to zero with increasing wavenumbers (e.g., Hisada [5][6]). To cope with this problem, we use the following wavenumber integrations for the integral of the first integrand of equation (11),

$$T_{ik}^D(X, Y; \omega) - T_{ik}^S(X, Y) = \int_0^\infty \{ t_{ik}^D(X, Y; \omega, k) - t_{ik}^S(X, Y; k) \} dk \dots \dots \dots (2)$$

where $t_{ik}^D(X, Y; \omega)$ and $t_{ik}^S(X, Y; \omega)$ are the dynamic and static terms of the integrands of the traction Green's functions, respectively. Since the dynamic integrand converges to the static integrand with

increasing wavenumber, the integrand of equation (2) attenuates rapidly, even for source points on free-surface. On the other hand, we employ the contour deformation method (Greenfield [7]) to evaluate the wavenumber integration of the static Green's functions in the second integration of equation (1). For more details, please see Hisada and Bielak [1].

Physical Interpretation of Fling Step and Directivity Pulse

Strike Slip Fault Model

Before investigating effects of sedimentary layers on near-fault strong motions, we briefly explain physics of the fling step and the directivity pulse using simple models embedded in a homogeneous half-space (Hisada and Bileak [1]). In particular, we pay special attention to the contribution of the static and dynamic terms of equation (1) to strong ground motions.

Fig. 3 shows a surface fault and a buried fault. They are the same left-lateral strike slip fault with 10 km x 5 km sizes. The maximum slip is 1 m including the top edges of the faults, and tapers at both side edges and at the bottom of the fault. The depths of the top of the faults are 0 km and 2 km, for the surface and buried faults, respectively. The slip velocity function is an isosceles triangle with a 1-second duration. The location of the hypocenter is shown in the figure, half way down the fault, and the rupture velocity is 2.5 km/s. The physical properties of the homogeneous half-space are $V_s = 2.5 \text{ g/cm}^3$, $V_p = 5 \text{ km/s}$, $V_s = 3 \text{ km/s}$, $Q_p = 200$, and $Q_s = 100$.

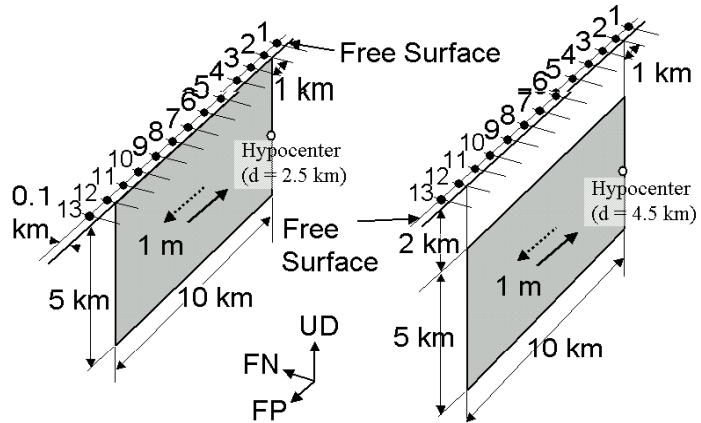
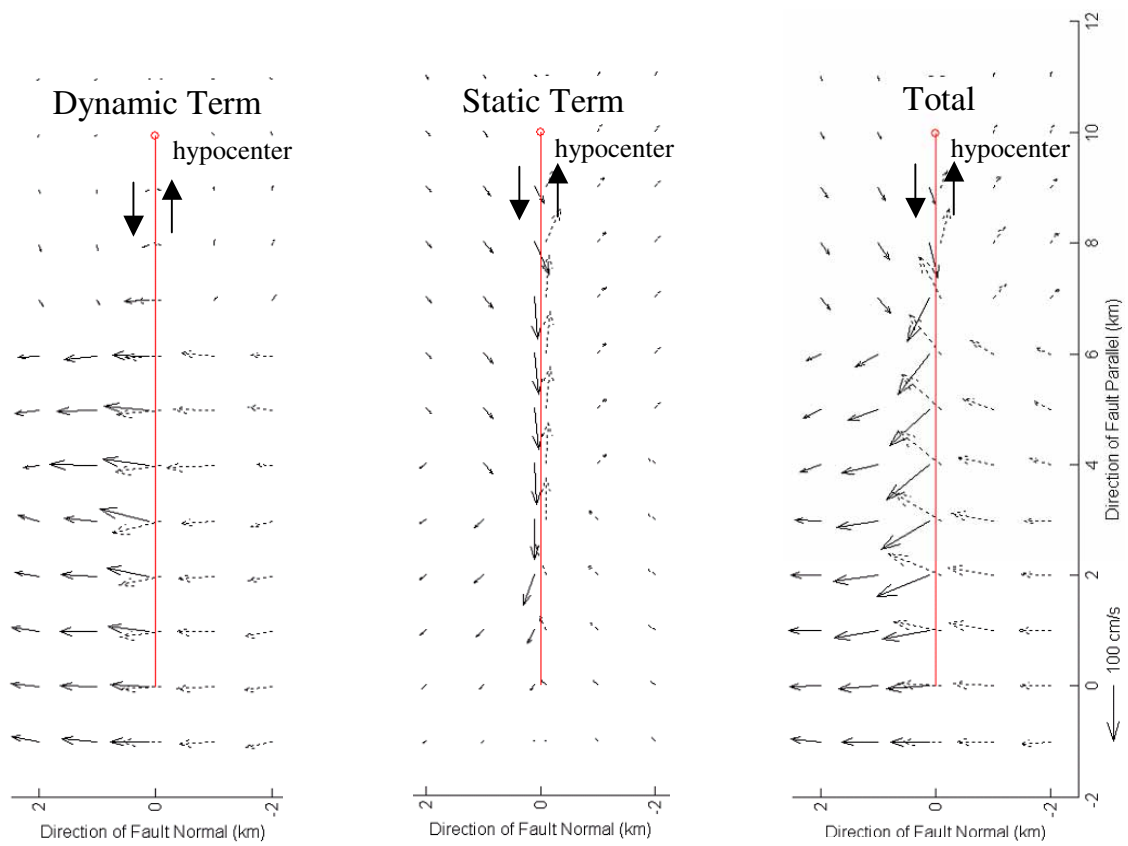


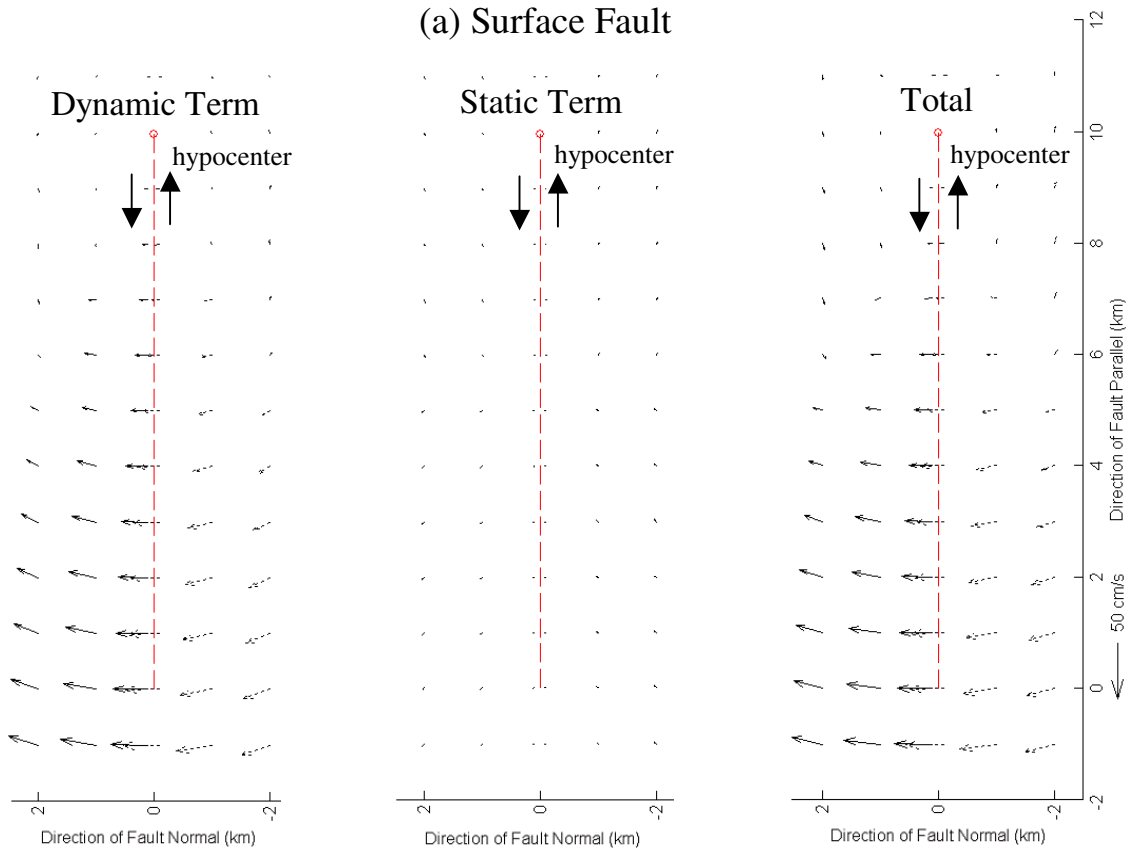
Fig.3 The surface fault model (left), and the buried fault model (right).

Results

Fig. 4 shows the vectors of the maximum velocities on the free surface using (a) the surface fault and (b) the buried fault. Both figures include three sets of waves on the line; the left and middle waveforms correspond to the dynamic and static terms, which stem from the first and second integrals in equation (1), respectively, and the rightmost panels represent the sums of the two terms. The amplitude scale for the buried fault is about half of that for the surface fault. The dynamic terms excite the directivity pulses in the fault normal components for both fault models, especially in the forward rupture direction (the lower half of the figures). By contrast, the static terms of the surface fault model generate large fling steps, *i.e.*, the large amplitudes in the fault parallel components in the vicinity of the fault. As the observation points get further from the fault, the static terms are quickly attenuated, whereas the dynamic terms are not. This is because the static terms consist of the static traction Green's function (*i.e.*, the order of attenuation is $1/r^2$), as seen equation (1), whereas the dynamic terms consist of the body and surface waves (*i.e.*, the order of attenuation is $1/r$ to $1/\sqrt{r}$). Therefore, the directions of the maximum velocities of the total waves are inclined with respect to the fault plane in the vicinity of the surface fault, because of the combined effects of the directivity pulses and fling steps. On the contrary, as for the buried fault model, the fling steps disappear and the directivity pulses are dominant. This is because in addition to the large attenuation of the fling steps, when an observation point is located above a buried fault, the slip dislocation of the fault cannot fling the ground, because of the presence of the continuous medium above the fault.



(a) Surface Fault



(b) Buried Fault

Fig.4 Vectors of maximum velocities on free surface for (a) the surface fault, and (b) the buried fault

EFFECTS OF SEDIMENTARY LAYERS ON DIRECTIVITY PULSE AND FLING STEP

Application to the 1992 Landers Earthquake

In order to investigate the effects of sedimentary layers on the directivity pulse and the fling step, we apply the above-mentioned method to a near-fault strong motion recorded during the 1992 Landers earthquake. Fig. 5 shows the fault model of the Landers earthquake by Wald and Heaton [2], and the observation station at the Lucerne valley. The fault model consists of the three left-lateral strike slip faults: the Camp Rock/Emerson fault (CEF), the Homestead valley fault (HVF), and the Johnson valley fault (JVF) from north to south. The right panel in Fig. 5 shows the sizes of the faults and their slip distribution. The station is about 2 km away from CEF, and is close to a large slip area of the fault (up to about 6 m). Table 1 shows the layered structure model used by Wald and Heaton [2].

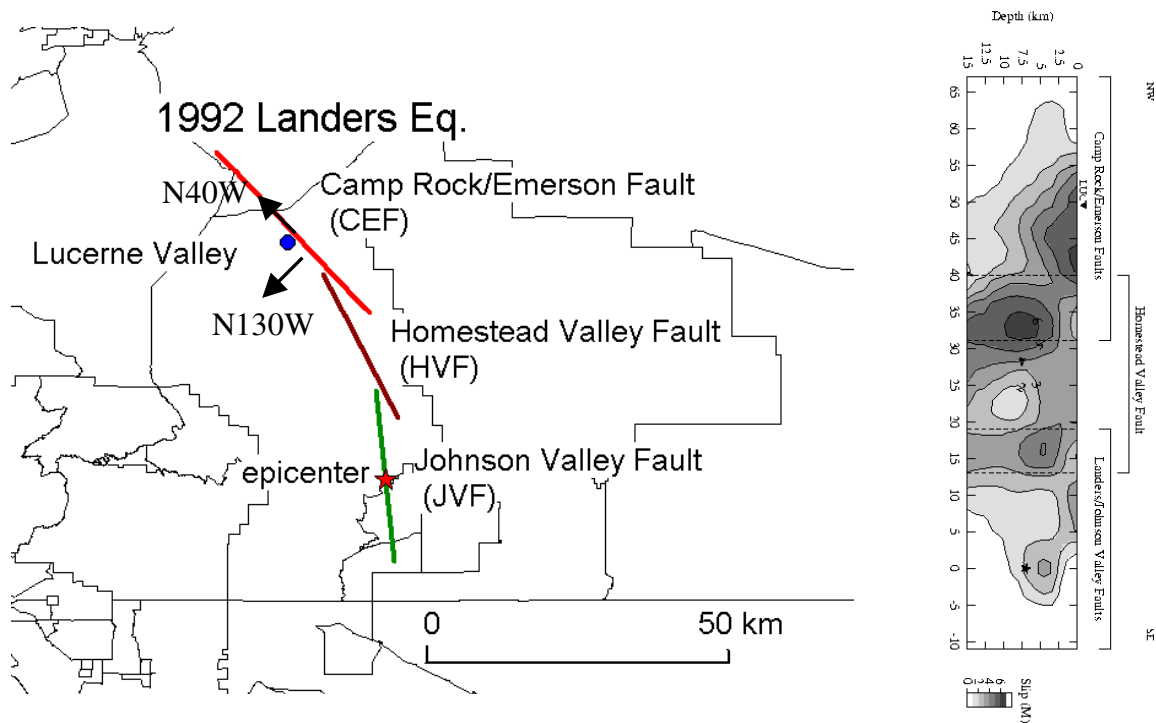


Fig.5 1992 The Landers earthquake model by Wald and Heaton [2], with the Lucerne valley station. The fault model consists of the three left-lateral strike slip faults: the Camp Rock/Emerson fault (CEF), the Homestead valley fault (HVF), and the Johnson valley fault (JVF). The right figure shows the slip distribution on the three faults (after Wald and Heaton [2])

Table 1 Layered Structure Model for the 1992 Landers Earthquake (Wald and Heaton [2])

Num.	Density (g/cm^3)	V_p (km/s)	Q_p	V_s (km/s)	Q_s	Thickness (km)
1	2.3	3.8	100	1.98	30	1.5
2	2.6	5.5	600	3.15	300	2.5
3	2.7	6.2	600	3.52	300	22.0
4	2.87	6.8	600	3.83	300	6.0
5	3.5	8.0	600	4.64	300	0.0

1-layer model
 4-layers model

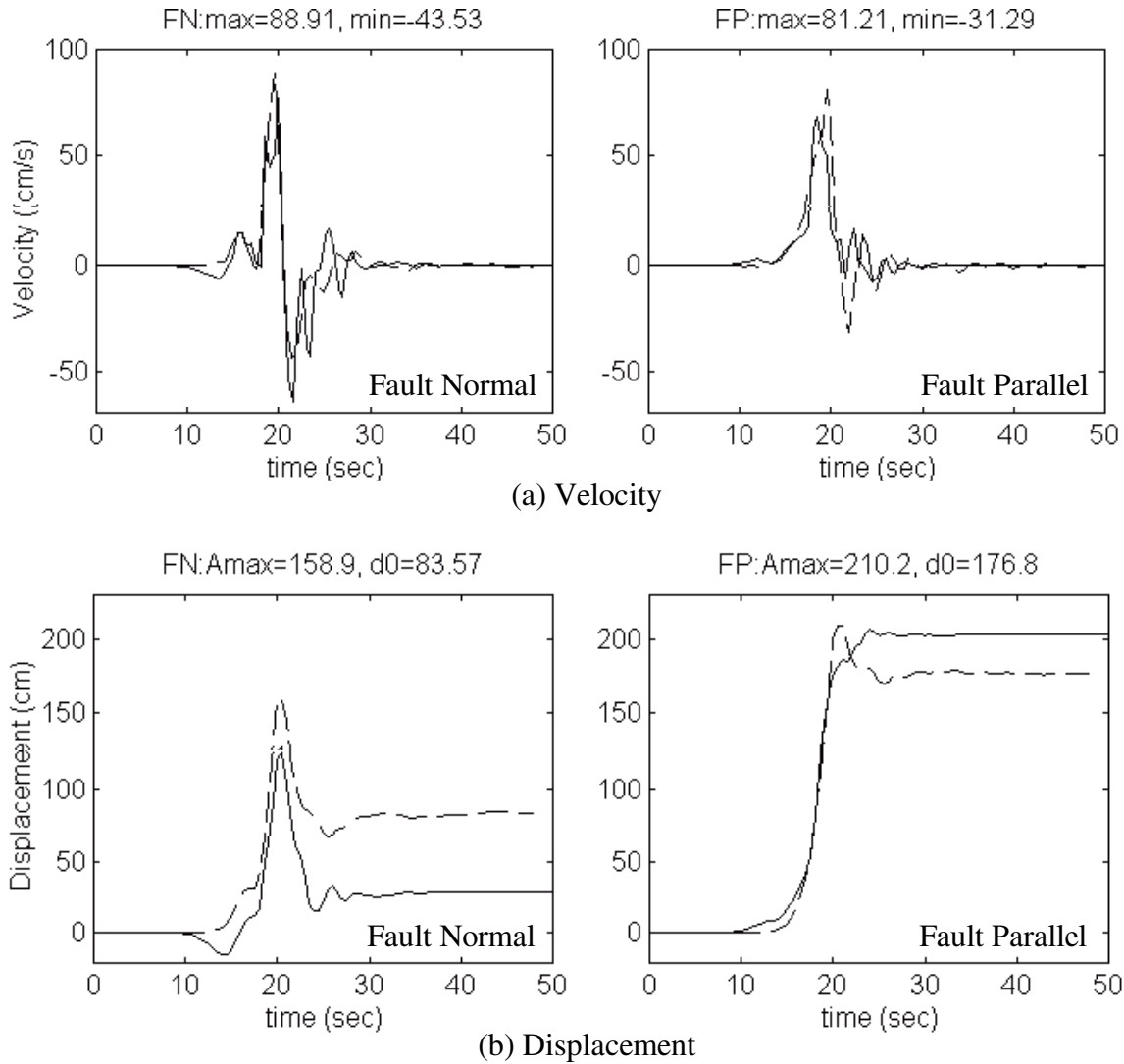


Fig.6 Comparisons between simulations (solid lines) and observations (dashed lines) at the Lucerne Valley station. The observed displacement records are corrected by Iwan [8].

Fig. 6 shows comparisons between simulations (solid lines) and observations (dashed lines) at the Lucerne Valley station, using a single layer on a halfspace; the observed displacement records are corrected by Iwan [8]. The fault normal and parallel components are N40W and N130W degrees, respectively (see Fig.5). The agreement between the simulated results and the observations is excellent, not only for the directivity pulses seen in the fault normal component, but also for the fling steps in the fault parallel component.

Fig. 7 shows the maximum velocities and displacements in the fault normal and parallel components, and the directions of the maximum values. In the figure, the first and second percentages in the parenthesis show the fractions of the dynamic and static terms, respectively. More than 90% of the fault normal velocity is composed of the dynamic term, whereas about 90% of the fault parallel displacement consists of the static term. As we have explained earlier, the combined effect of the directivity pulse and the fling step makes the directions of the maximum amplitudes inclined to the fault plane, about 41 and 36 degrees from the fault plane for the simulated velocity and displacement, respectively. Those values are fairly close to the observations, 48 and 38 degrees, respectively.

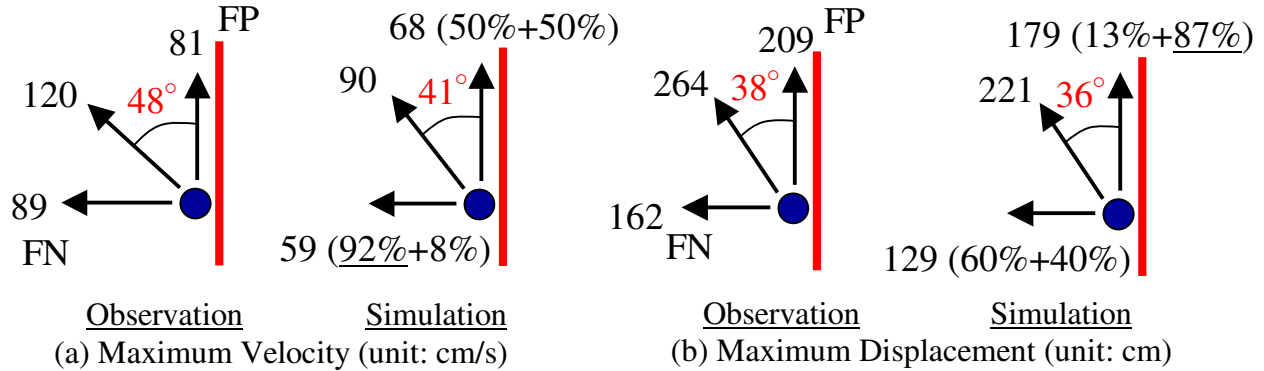


Fig.7 The maximum (a) velocities and (b) displacements in the fault normal and parallel components at the Lucerne valley station, and the directions of the maximums and those values. The first and second percentages in parenthesis show the fractions of the dynamic and static terms, respectively.

Effects of Sedimentary Layer on Directivity Pulse and Fling Step

We will check the effects of the sedimentary layer on the strong motion at the Lucerne valley station. In the following calculations, we use three layered structure models shown in Table 1. The first model is the original five-layered model, and the second is a homogeneous half-space model, whose material properties are those of Num. 3 in Table 1. The last is a 4-layered model, whose structure is the same as that of Table 1 except that the top sedimentary layer has been removed. In addition, we will also check the contribution of the three faults: CEF, the nearest fault (about 2 to 20 km), HVF, the middle fault (about 8 to 35 km), and JVF, the furthest fault (about 30 to 55 km) to the station (see Fig.5).

Figs 8(a) and (b) show the velocities and displacements simulated using CEF, the closest fault. Both figures include three sets of waves; the middle and right waves correspond to the dynamic and static terms, which stem from the first and second integrals in equation (1), respectively. The leftmost waves represent the sums of the two terms. As in the previous simple model, the dynamic term excites directivity pulses in the fault normal component, whereas the static term generates a very large fling step (up to about 1.8 m) in the fault parallel component. The static term dominates over the dynamic term in the fault parallel displacement. As for the effects of the sedimentary layer, the larger waves with longer duration can be seen in the 5-layered model in the directivity pulses than those of the 1- and 4-layered models. Clearly, these waves are the body and surface waves excited in the sedimentary layer. On the contrary, we cannot see big differences in the fling step (*i.e.*, the static term) among the three layered structure models. This is because the fling step is dominated by the slip of the nearest fault, about 2 km in this case.

Similarly, Figs 9(a) and (b) show the velocities and displacements, respectively, simulated using HVF, the middle distance fault. The amplitudes of the directivity pulses are still comparable with those of CEF, about 70 cm/s of velocities, as seen in the fault normal components in Figs. 8(a) and 9(a). However, the fling steps become much smaller than those of CEF, as seen in the static displacements of the fault parallel components of Figs. 9(b) and 8(b) (*i.e.*, 30 cm for HVF and 170 cm for CEF). Again, much larger waves with longer duration are seen in the 5-layered model in the dynamic terms than those of the 1- and 4-layered models. By contrast with CEF, some differences can be seen in the amplitudes of the static terms among the three layered models, especially in the displacements. This is probably due to the long distance in the highly attenuated (*i.e.*, the low-Q value) sedimentary layer. Honda [9] reported similar results by comparing a homogenous model and a layered model.

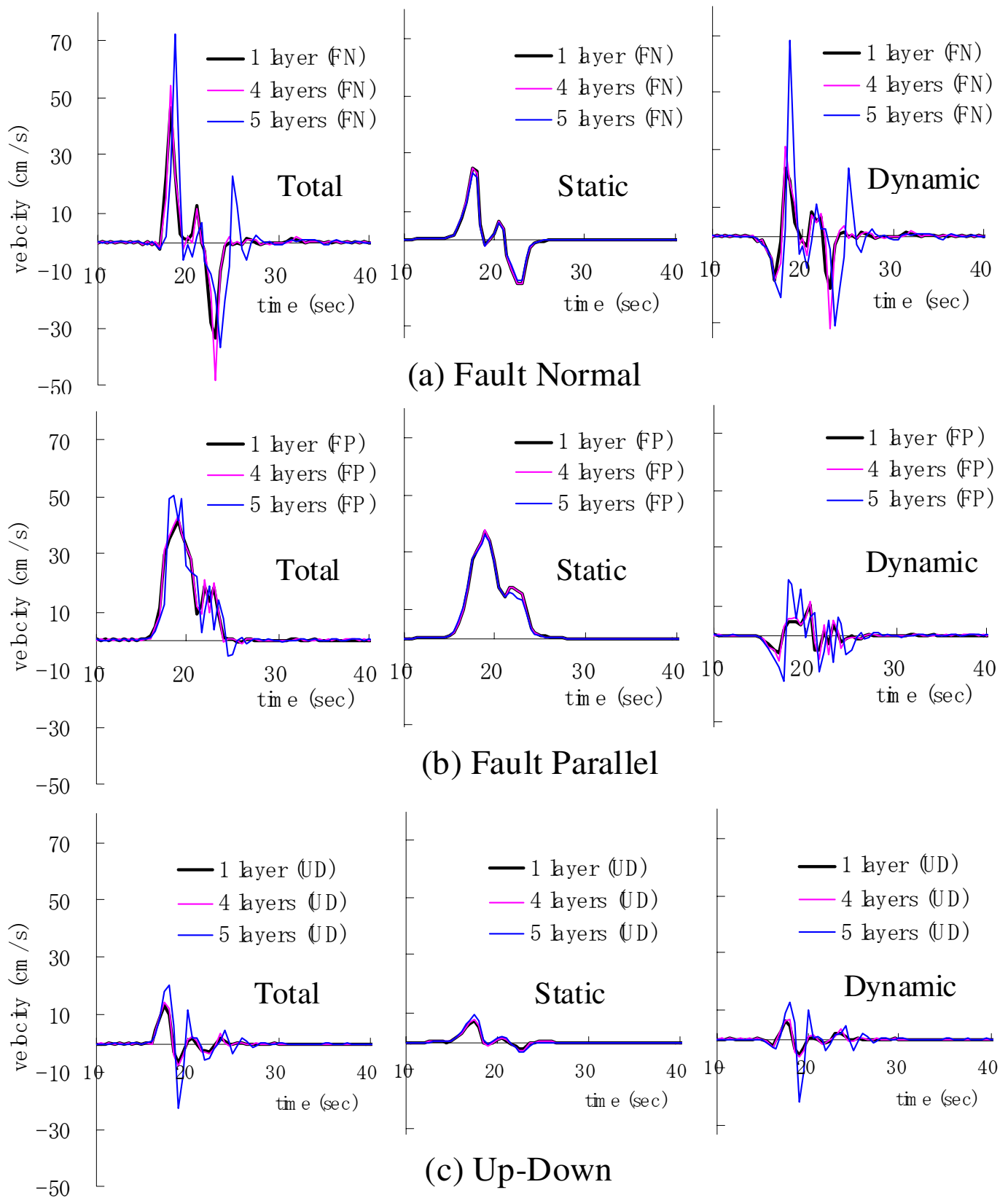


Fig.8(a) Velocities simulated at the Lucerne Valley site using the Camp Rock/Emerson fault model (CEF)

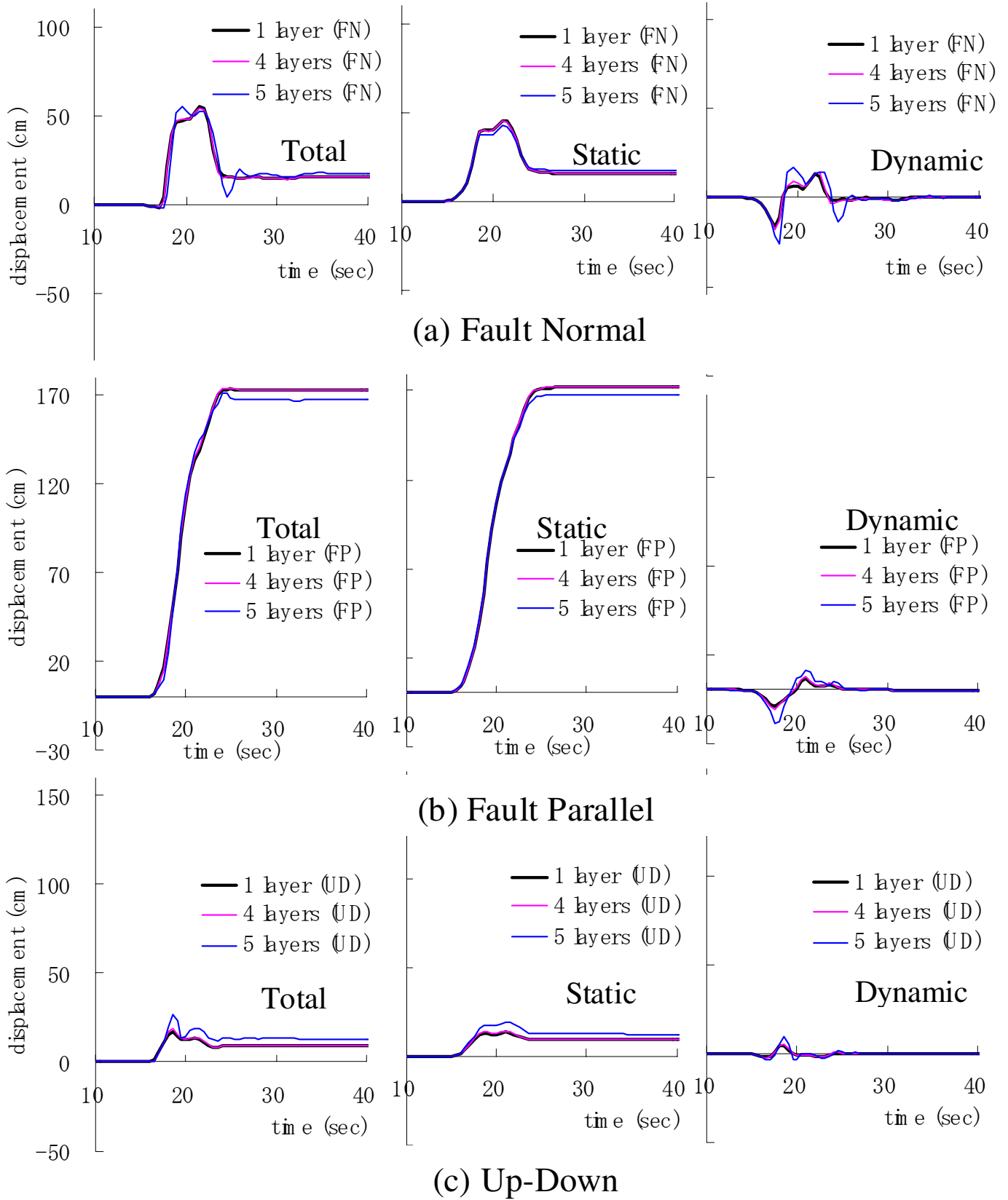


Fig.8(b) Displacements at the Lucerne Valley site using the Camp Rock/Emerson fault model (CEF)

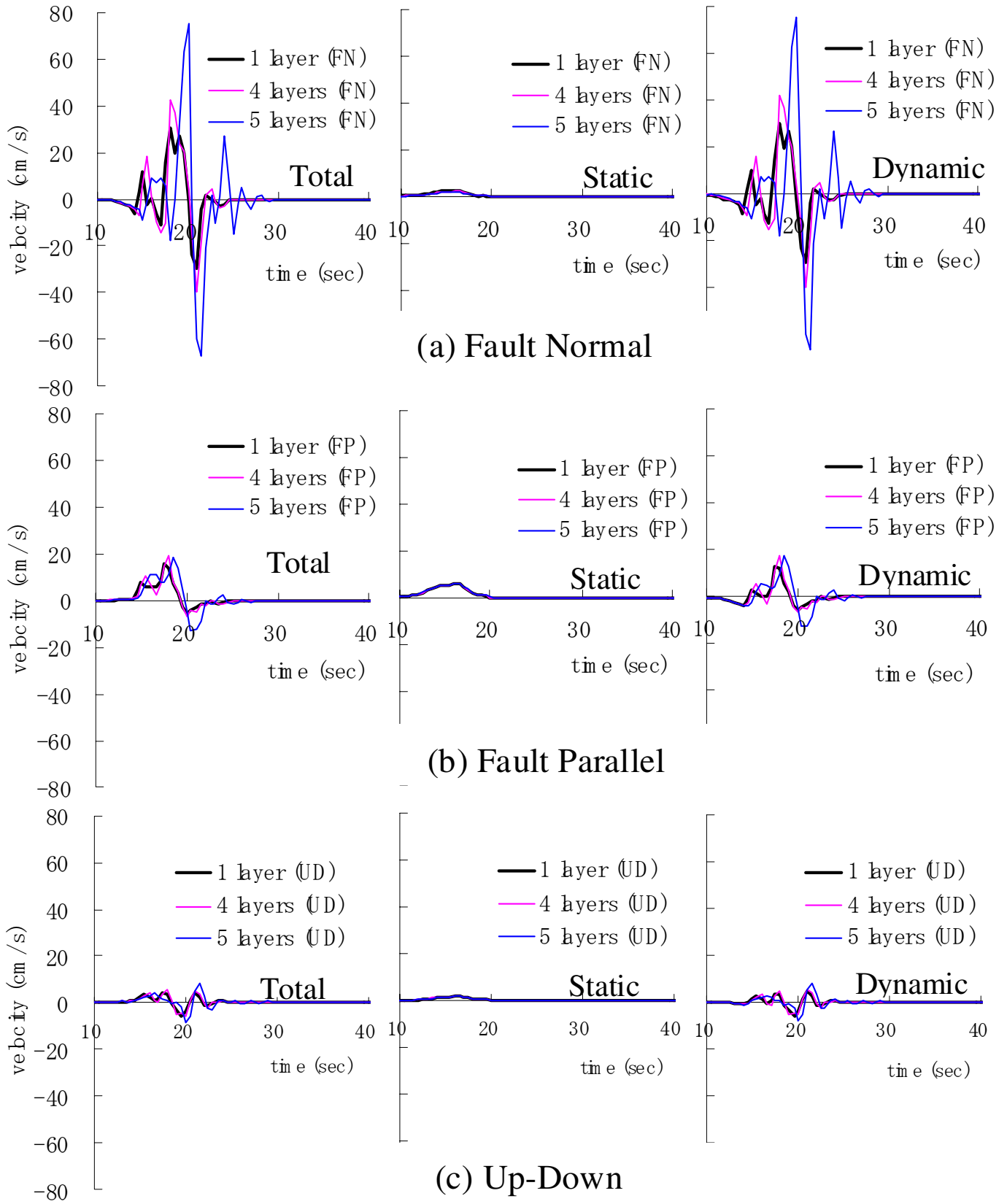


Fig 9(a). Velocities simulated at the Lucerne Valley site using the Homestead Valley fault model (HVF)

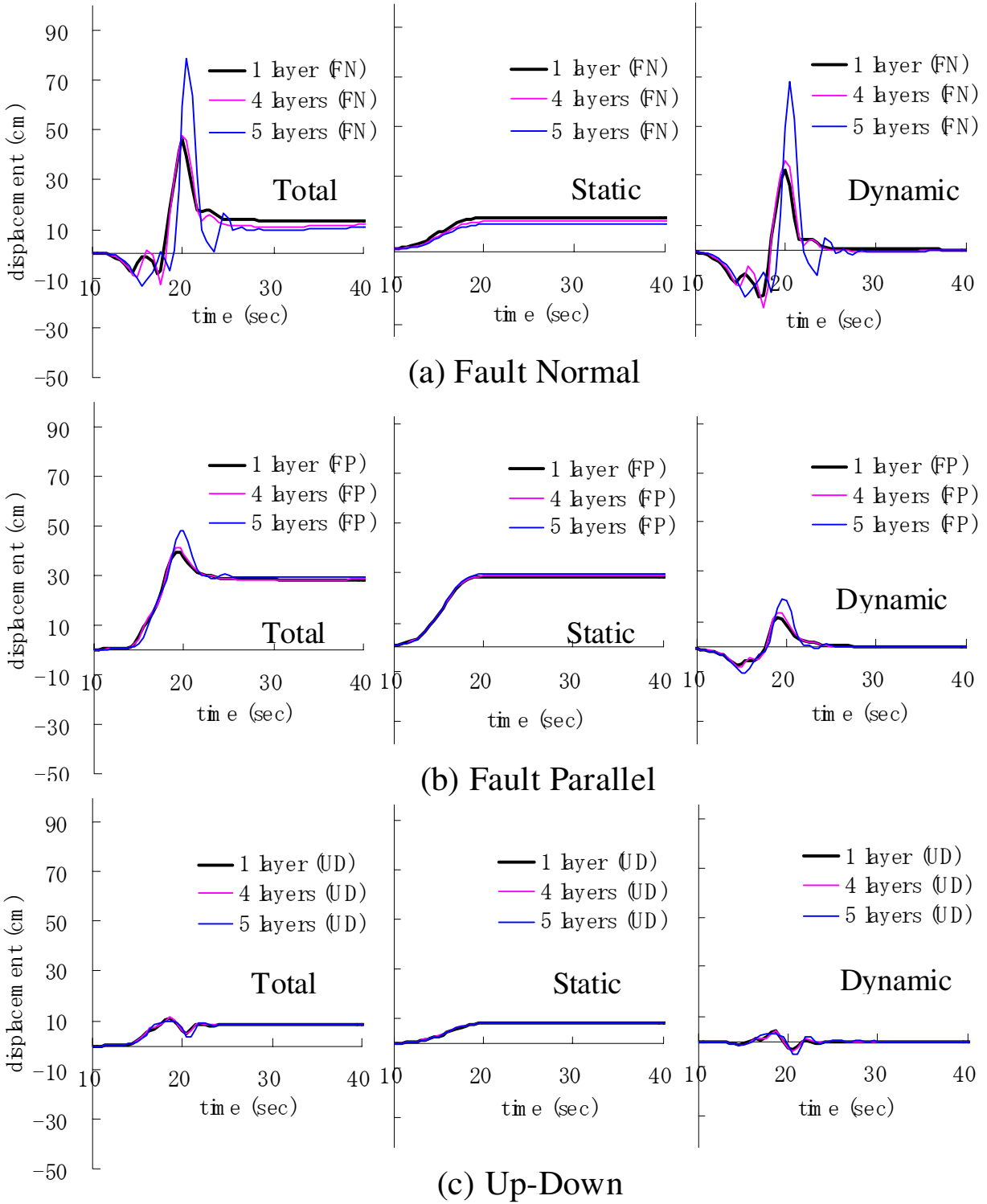


Fig.9(b) Displacements at the Lucerne Valley site using the Homestead Valley fault model (HVF)

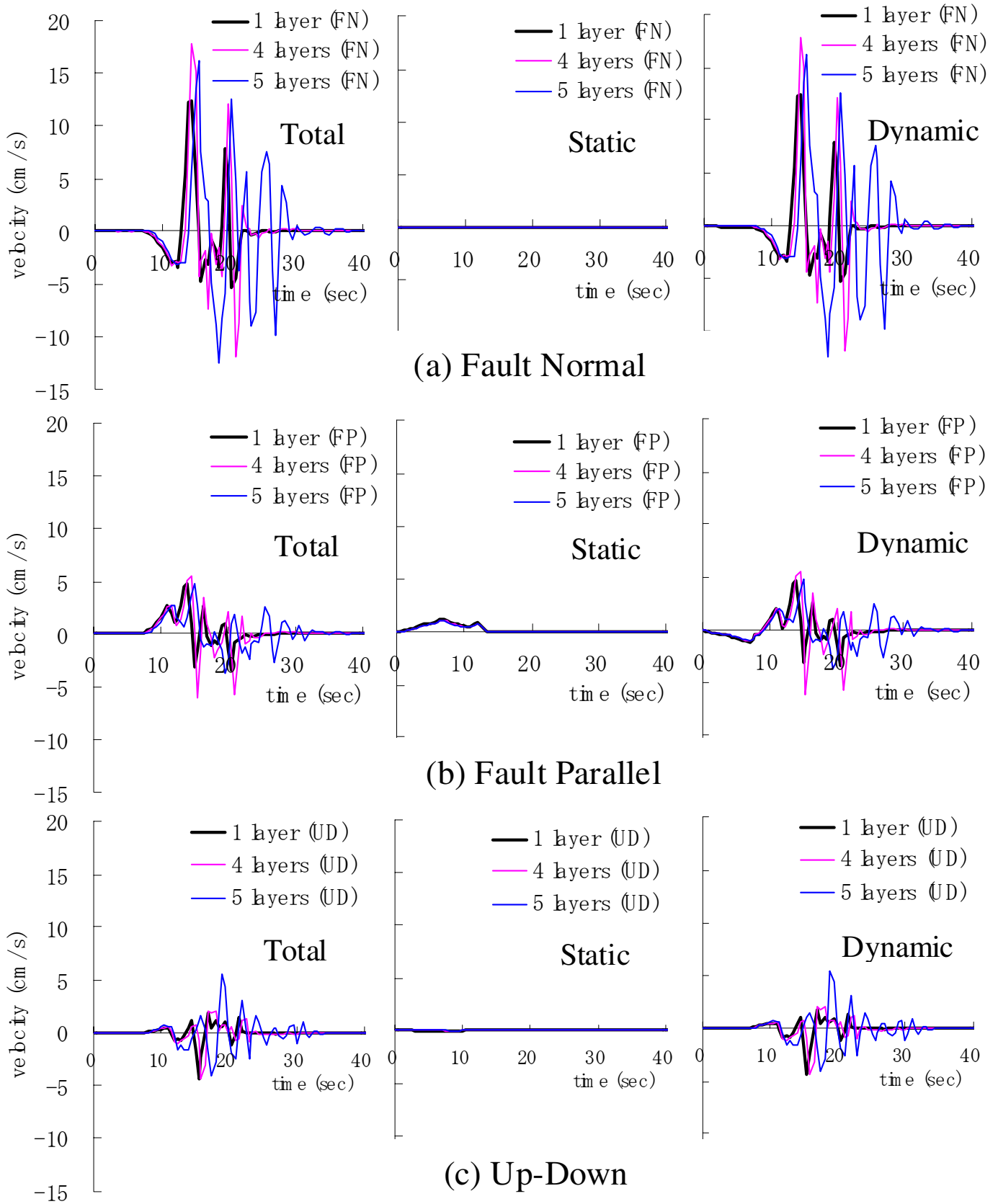


Fig.10(a) Velocities simulated at the Lucerne Valley site using the Johnson Valley fault model (JVF)

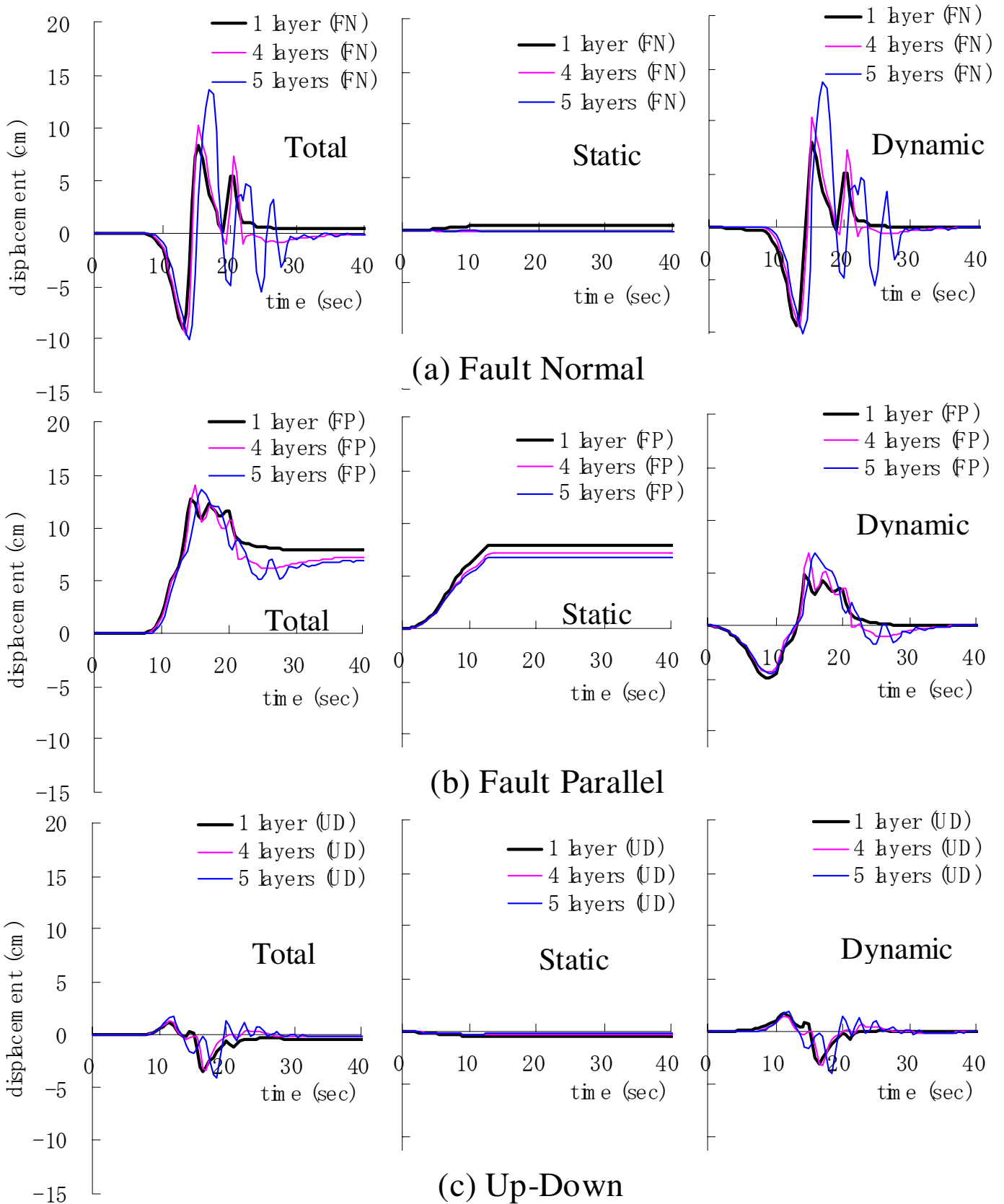


Fig.10(b) Displacements simulated at the Lucerne Valley site using the Johnson Valley fault model (JVF)

Finally, Figs. 10(a) and (b) show the velocities and displacements, respectively, simulated using JVF, the furthest fault. Even though we still see the fling step in the fault parallel displacements, the directivity pulses are dominant over the fling steps, especially in the fault normal velocities. The amplitudes of the pulses are largely attenuated as compared with those CEF and HVF (about one fourth). Again, larger waves with longer duration are seen in the 5-layered model in the dynamic terms than those of the 1- and 4-layered models. The differences of the static terms among the three models are more clearly seen than those of CEF and HVF, as seen in the displacements of Fig. 10(b). This is again due to the longer distance in the low-Q sedimentary layer.

CONCLUSIONS

We investigated the effects of sedimentary layers on the long-period directivity pulse and the fling step using the theoretical method (Hisada and Bielak [1]). After checking the basic physics of those waves, we applied the method to the strong motion recorded at the Lucerne valley during the 1992 Landers earthquake. We confirmed that the combined effect of the long-period pulse and the fling step made the maximum amplitude of the velocity and displacement inclined to the fault plane at 30 – 50 degree. We found that the inclusion of sedimentary layers increased greatly the amplitudes and durations of the directivity pulses, whereas it did not affect significantly the directivity pulse. This is because the directivity pulses are excited from the wide range of the faults including the nearest to the furthest fault, whereas the fling steps are mostly generated by the slip of the nearest fault.

ACKNOWLEDGMENT

This research was partly supported by a special project of US-Japan Cooperative Research for Urban Earthquake Disaster Mitigation (No.11209201), Grant-in-Aid for Scientific Research on Priority Area (Category B), Ministry of Education, Culture, Sports, Science and Technology of Japan (MEXT), and Earthquake and Environmental Research Center of Kogakuin University funded by the Frontier Research Promotion Program of MEXT (Y.H.). This work was also supported by the National Science Foundation KDI program, under grant CMS-9980063 (J.B.); the cognizant program director is Clifford Astill. We are grateful for this support. We obtained the strong motion records used in this study from COSMOS Virtual Data Center.

REFERENCES

1. Hisada Y, Bielak J, “A Theoretical Method for Computing Near-Fault Strong Motions in Layered Half-Space Considering Static Offset due to Surface Faulting, with a Physical Interpretation of Fling Step and Rupture Directivity”, *Bull. Seism. Soc. Am.*, *93*, 1154-1168, 2003.
2. Wald DJ, Heaton TH, “Spatial and temporal distribution of slip for the 1992 Landers, California earthquake”, *Bull. Seism. Soc. Am.*, *84*, 668-691, 1994.
3. Somerville PG, Smith NF, Graves RW, Abrahamson NA, “Modification of empirical strong ground motion attenuation relations to include the amplitude and duration effects of rupture directivity”, *Seismological Res. Letter*, *68*, 199-222. 1997.
4. Abrahamson, N, “Incorporating effects of near fault tectonic deformation into design ground motions”, a presentation sponsored by EERI Visiting Professional Program, hosted by the University at Buffalo, October 26, 2001 (<http://mceer.buffalo.edu/outreach/pr/abrahamson.asp>).

5. Hisada Y, "An efficient method for computing Green's functions for a layered half-space with sources and receivers at close depths", *Bull. Seism. Soc. Am.*, *84*, 1456–1472, 1993.
6. Hisada Y, "An efficient method for computing Green's functions for a layered half-space with sources and receivers at close depths (Part 2)", *Bull. Seism. Soc. Am.*, *85*, 1080-1093, 1995.
7. Greenfield RJ, Comments on "An efficient method for computing Green's functions for a layered half-space with sources and receivers at close depths" by Y. Hisada, *Bull. Seism. Soc. Am.*, *85*, 1523-1524, 1995.
8. Iwan WD, Corrected Accelerogram, 1992 Landers earthquake, COSMOS Virtual Data Center (<http://db.cosmos-eq.org/>).
9. Honda R, Yomogida K, "Effects of a soft surface layer on near-fault static and dynamic displacements", *Geophys. J. Intern.*, *154*, 441-462, 2003.